Modeling the aging effects due to bubble coverage at the electrode in Anion Exchange Membrane Water Electrolysis

Ronit-Kumar Panda, Guillaume Serre, Frederic Fouda-Onana, Yann Bultel, Pascal Schott, Johannes Ast

A0208

Modeling the aging effects due to bubble coverage at the electrode in Anion Exchange Membrane Water Electrolysis

Ronit Kumar Panda (1), Guillaume Serre (1), Frederic Fouda-Onana (1), Yann Bultel (2), Pascal Schott (1), Johannes Ast (1)
(1) Univ. Grenoble Alpes, CEA, LITEN, DEHT, F-38000 Grenoble, France;
(2) Univ. Grenoble Alpes, Univ. Savoie Mont Blanc, CNRS, Grenoble INP, LEPMI, F-38000 Grenoble, France
ronit-kumar.panda@cea.fr

Abstract
This focuses on the decline in performance induced by the loss of wettability in the anode Porous transport layer (PTL) due to extended bubble coverage. We performed a series of multiple potentiometric tests including breaks every 10 hours combined with Electrochemical Impedance spectroscopy. Using this protocol, we obtain the variation in reaction Kinetics, Ohmic resistance and evolution of mass-transfer limit in the Anion Exchange Membrane Water Electrolysis (AEMWE). Our goal was to study the evolution of concentration overpotential in the AEMWE due to the variation in wettability. Our methodology was to characterize the two-phase flow properties in the PTL that plays a key role in the concentration overpotential at the electrode. It was performed using flow simulations with Geodict using 3D tomographic images of the Stainless steel (SS) PTL at the anode. These simulations were performed at the beginning of durability tests and the properties at the end of life were determined using a modified contact angle. We obtain the effective permeability of the medium to be implemented in the Darcy law as well as the capillary pressure at the electrode, for beginning and end of durability tests. Subsequently, these properties were implemented in our performance code to simulate the polarization curves at the beginning and end of life.

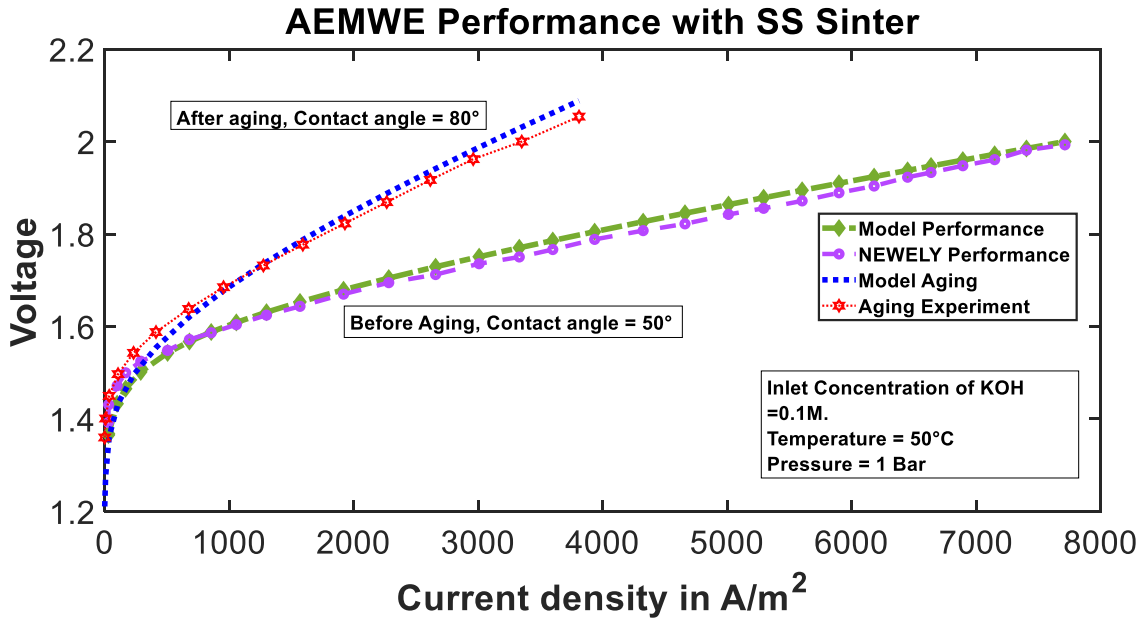

Figure 1 Polarisation curves for the AEM Water electrolyser at the beginning and end of stability tests with liquid electrolyte fed at the anode.

Acknowledgement - This project has received funding from the Fuel Cells and Hydrogen 2 Joint Undertaking under grant agreement No 875118. This Joint Undertaking receives support from the European Union's Horizon 2020 research and innovation program, Hydrogen Europe and Hydrogen Europe research.

Introduction

Anion exchange membrane water electrolyzers (AEMWEs) have shown great potential as an alternative to traditional proton exchange membrane water electrolyzers due to their lower operating temperatures and potentials and the use of non-noble catalyst. However, the aging degradations and the life time of such electrolyzer are not well known and must be studied for industrial applications. One of the major causes of irreversible aging in AEMWEs is the loss in wettability of the Porous Transport layer (PTL) at the anode.[22] When the PTL becomes less hydrophilic or even hydrophobic, the contact between the catalyst layer and the electrolyte decreases, leading to a decrease in performance and eventually, the failure of the electrolyzer. Therefore, understanding the mechanism of wettability loss and developing strategies to mitigate it is crucial for the long-term stability and performance of AEMWEs. In this paper, we investigate the effect of wettability loss at the anode PTL of AEMWEs, and propose a method to quantify the degree of wettability loss using electrochemical impedance spectroscopy. [1][2][3]

1. Model Development

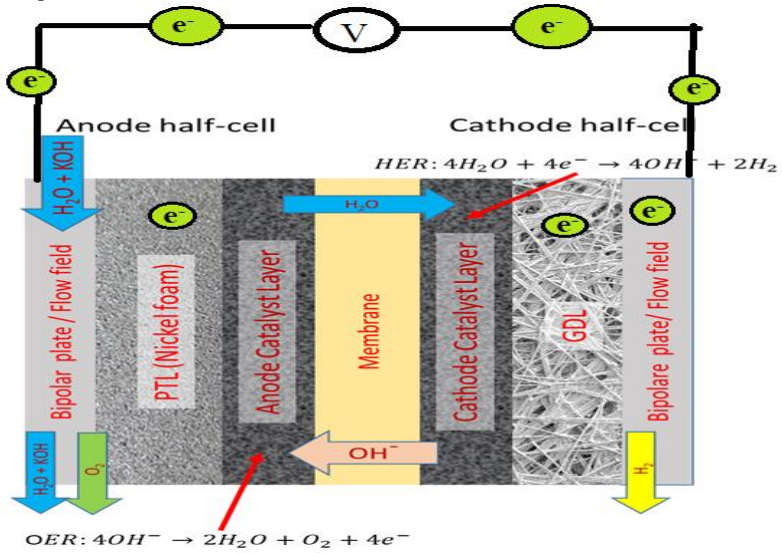

Figure 1 Schematic of the Anion exchange membrane based Water electrolyzer

The performance of Anion exchange membrane based water electrolyser (AEMWE) heavily relies on the efficient transport of reactant gases to the catalyst layer and the effective removal of gas products from the catalyst layer. For the scope of this paper, we consider Gas diffusion electrodes as a combination of Porous Transport Layers and Electrode Layers at the anode. [4] In our previous work, we discussed the use of anion exchange membrane (AEM) electrolysis for hydrogen generation and explored the effects of adding Potassium Hydroxide (KOH) to the water feedstock [5]. In an extension of the performance model presented in the previous paper, this study focuses on investigating the loss in wettability of the anode porous media in an anion exchange membrane-based water electrolyser. [6]

1.1 Performance Limitations in the AEMWE

Table 1 Phenomenon involved in the AEMWE and the associated device component

Phenomenon	Domain

Electro-migration, diffusion of ion and streaming potential driven by the chemical potential gradient of water ($\eta_{membrane}$)	**AEM**
Electronic resistance of the Anode PTL, Cathode GDL (η_{ohm})	**PTL and GDL**
Alkaline media influence on the kinetics at low pH (η_{pH})	**Catalyst layer interface**
Ion exchange Overpotential ($\eta_{ion-exchange}$)	**Liquid electrolyte - ionomer interface**
Activation Overpotential at the electrodes ($\eta_{cat} + \eta_{an}$)	**Catalyst interface**

A schematic of the AEMWE is presented in the **Figure 1**. In the **Table 1**, we also list the key phenomenon that result in the device overpotential and hence warrant a thorough understanding and study. The overall cell voltage is calculated based on **Equation 1**.

$$U_{cell} = U_0 + K(T - T_{ref}) + \frac{RT}{nF} \ln \frac{a_{H_2} a_{O_2}^{0.5}}{a_{H_2O}} + \eta_{cat} + \eta_{an} + \eta_{ohm} + \eta_{ion-exchange} + \eta_{pH} + \eta_{membrane} \quad (1)$$

where η_{cat} , η_{an} are the activation overpotential at the cathode and anode respectively. η_{pH} is the overpotential due to the pH gradient through the membrane. The overpotential due to the Ohmic resistance (η_{ohm}) of the electrolyser components (electrical resistances of anode and cathode PTL and GDL and contact resistances), and $\eta_{ion-exchange}$ refers to the overpotential resulting from the ion transport between the ionomer and liquid electrolyte. $\eta_{membrane}$ Refers to the overpotential due to the resistance in transport of ions in the AEM. For the scope of this work, we will not delve deeply into the determination of AEMWE overpotential and details of the modelling using our AEM electrolyzer code developed in Matlab/Simulink: MePHYSTO. This macroscopic code is 1D through-plane and 1D in-plane. It has been extensively described in our previous work. [5] In the field of fuel cells and electrolysis, it is common to observe a reference pressure of one bar to express the activity of species in the literature. However, we divide the partial pressure of water and other species by the saturation pressure of water ($P_{saturation}$), which is the pressure at which water transitions between liquid and vapor phases at a given temperature. It ensures that the relative pressures and activities are properly scaled and consistent within the system. By dividing the partial pressures of Hydrogen(P_{H_2}) , Oxygen (P_{O_2}) and Water (P_{H_2O}) by the saturation pressure, we obtain a ratio that represents the degree of water saturation or relative humidity in the domain. [7]

The gases and water activities are then determined as: -

$$a_{H_2} = \frac{P_{H_2}}{P_{reference}}, a_{O_2} = \frac{P_{O_2}}{P_{reference}}, a_{H_2O} = \frac{P_{H_2O}}{P_{saturation}} \quad (2)$$

In our work, we used a modified Butler-Volmer kinetics at each electrode:-

$$\eta_{cat,an} = \frac{RT}{\alpha_{c/a} F} \operatorname{arcsinh}\left(\frac{i}{2\, i_{0,cat/an}}\right) \quad (3)$$

where $\alpha_{a/c}$ is the symmetry factor, (0.5 in this case) and $i_{0,an}$ and $i_{0,cat}$ refer to the anode and cathode exchange current density given by:

$$i_{0,\frac{an}{cat}} = i_{0,ref}\ \gamma_{\frac{an}{cat}}\ \exp\left(\frac{-E_{c\frac{an}{cat}}}{R}\left(\frac{1}{T} - \frac{1}{T_{ref}}\right)\right) \quad (4)$$

$i_{0,ref}$ being the reference exchange current density per unit catalyst area, $E_{c\frac{an}{cat}}$ is the activation energy (J/mol), and T is the operating temperature).[8][9] The roughness factor

($\gamma_{\frac{an}{cat}}$), which is a measure of the surface area of the electrode in contact with the electrolyte, can have a significant effect on the reaction kinetics. In our model it is a function of the liquid saturation (s_L) catalyst density (ρ_c), catalyst loading (a_c) and the crystallite diameter (D_c). Note that $\gamma_{\frac{an}{cat}}$ is electrode roughness factor the reactions at the respective electrodes. Liquid saturation (s_L) refers to the fraction of pore space occupied by the liquid phase, while gas saturation (s_G) represents the fraction occupied by the gas phase. These saturation values play a vital role in determining the flow distribution of the two phases within the porous structure.

$$\gamma_{\frac{an}{cat}} = = \emptyset\, a_c\ L_c\ s_L\ \frac{6}{\rho_c\ D_c} \quad (5)$$

The roughness factor was deduced using the Equations 3-5 from the available IV Curves from various experiments, at an operating temperature, electrolyte concentration and pressure.

1.2 Ion exchange Overpotential

The ion exchange overpotential is a complex contribution to the potential, which is why it is necessary to describe it in details.

The three primary transport pathways for ions in AEMWE are:

1. Bulk transport refers to the motion of ions through the bulk of the membrane.
2. Interfacial transport refers to the motion of ions across the interface between the membrane and the electrode. This pathway is important for ion transport in the immediate vicinity of the electrode.
3. Ionomer liquid electrolyte transport refers to the motion of ions through the ionomer liquid electrolyte that connect the membrane to the electrode.

The Ion exchange at the electrodes overpotential is calculated from Equations 6 and 7:

$$\Delta\eta_{ion-exchange} = \frac{1}{i_{cell}}\ \delta\left(R_{exchange} F(\eta_{membrane} - \eta_{electrolyte})\right) \quad (6)$$

$$R_{exchange} = k_{exchange}\left(c_{OH^-}^{membrane}\ exp\left(\frac{z_i F(\eta_{membrane} - \eta_{electrolyte})}{RT}\right) - c_{OH^-}^{electrolyte}\right) \quad (7)$$

However, the Donnan overpotential and the ion exchange overpotential are often used interchangeably in the literature, so it is important to clarify that they arise from distinct processes and have different characteristics. The Donnan overpotential results from an imbalance in ion concentrations across the ionomer-liquid electrolyte interface, leading to the establishment of an electro-static potential difference to maintain charge neutrality. On the other hand, the ion exchange overpotential specifically refers to the overpotential associated with the transfer of ions at the ionomer-liquid electrolyte interfaces. It arises from the resistance encountered by ions as they move through the ionomer layer and exchange with the ions in the liquid electrolyte. The relatively lower significance of the Donnan overpotential in AEM-based electrolyzers can be attributed to its dependence on the concentration and mobility of counterions near the AEM. In contrast, the ion exchange overpotential, which is typically more dominant, is influenced by factors such as ion transport resistance, solution conductivity, and diffusion limitations. Therefore, the ion exchange overpotential takes precedence over the Donnan overpotential in determining the overall performance of AEM-based electrolyzers. [10][11][12][17][18]

1.3 Darcy Two phase flow modelling in AEMWE

The two-phase mass transport in the porous media are modelled by the Darcy two-phase flow equation in MePHYSTO. The parameters involved in this Darcy law are the following ones: the absolute permeability (K) characterizes the porous medium's ability to transmit fluids and is a measure of its intrinsic properties. Relative permeability ($k_{r,g,l}$) describes the effective permeability of a specific phase (liquid or gas) in the presence of another immiscible phase.[13] In the **equation 6**, $u_{g,l}$ is the velocity of the gas and liquid phase respectively:

$$u_{g,l} = -\frac{K\, k_{r,g,l}}{\mu_{g,l}} \operatorname{grad}(P_{g,l}) \quad (8)$$

K, $k_{r,g}$, $P_{g,l}$and μ_g denoting the absolute permeability of the porous medium, the relative permeability, the pressure gradient and the viscosity for the gas and liquid, respectively. Note that the relative permeability of the liquid is a function of the water saturation (s_L) like in **Equation 7** that is a law frequently used.

$$k_{r,l} = (s_L)^3 \quad (9)$$

The pressure difference between the gas phase and liquid phase is related to the capillary pressure (P_c), which is the pressure difference across the liquid-gas interface. It is a function of surface tension (σ), the liquid saturation(s_L) at the electrodes and a length scale (L) often associated to the porosity and permeability. J(s) is the Leverett function that involves the liquid saturation, providing insights into phase displacement and distribution in the porous medium. Another key modelling parameter is the contact angle (θ_c) which is the angle formed between the liquid phase and the solid surface. [14] [15] [16][19][20]

$$P_c = \frac{\sigma \cos(\theta_c)}{L} J(s) \quad (10)$$

$$s_G + s_L = 1 \quad (11)$$

$$P_c = \sigma \cos(\theta_c) \left(\frac{\epsilon}{K}\right)^{0.5} J(s) \quad (12)$$

2. Impact of the loss of wettability of the PTL on the electrolyzer performances

In the experimental study, the MEAs were CCS like with Nickel foam as PTL and a GDL (H23C7 from Freudenberg) as cathode GDL. The single cell tests were carried out in a 2-cm² geometrical electrode surface in 0.1 M KOH at 50°C and atmospheric pressure. The electrolyte was supplied on the anode side of the cell with a flowrate of 500 ml/min and there was no electrolyte fed to the cathode. During 10 periods of 10 hours, the potential was maintain constant and equal to 2V in order to promote aging effects. At the beginning of life and between each period, the High and Low frequency resistances were measure using Electrochemical Impedance spectroscopy and the IV curves have been recorded.

The model Validation workflow is described as follows:
1. The 3D tomographic images of the PTL used in the aging studies have been recorded at CEA. These images were processed, rendered and segmented using GEODICT.
2. The absolute permeability was calculated from the above images provided to GEODICT using the Flowdict module. The input parameters were the fluid and flow properties such as the inlet flowrate of the electrolyte and the flow direction. Quasi-static pore morphology method was used and it was assumed that the material is homogeneous i.e we realize that

there is a well-defined contact angle between the PTL surface and phase boundaries throughout the computational domain.
3. The relative permeability vs. saturation was obtained using the Satudict module of GEODICT. The contact angle as input of this calculation plays a crucial role in defining the wetting behavior. The relative permeability was determined for several values of the contact angle, assuming it varies during the ageing.

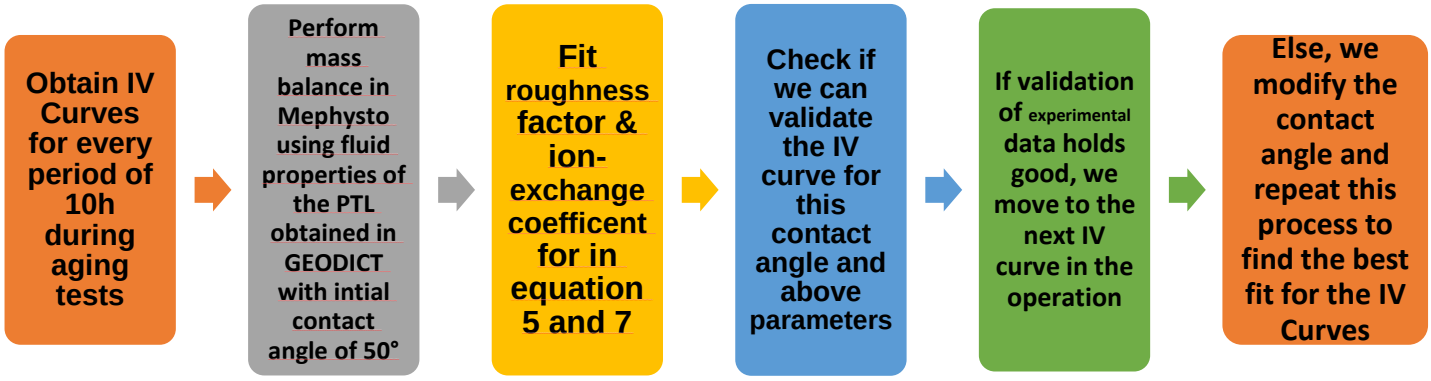

Figure 2 Workflow of the model presented in this work.

2.1 Results and Discussion

Table 2 Experimental parameters used in this study

Symbol	Value
Membrane thickness (microns)	180
ACL thickness (microns)	80
CCL thickness (microns)	60
Anode Porous Transport layer(microns)	480
Cathode Gas diffusion layer(microns)	230
Operating Temperature in Kelvin	323.15
Operating Pressure in bar	1

Over an extended aging period as seen in **Figure 3**, the IV curves exhibit distinct characteristics that can be attributed to the effects of irreversible degradation for all values of current, indicating that electrochemistry and fluid transport are affected by the degradations. Initially, the IV curves indicate efficient electrochemical kinetics and good wettability between the electrolyte and electrodes. However, as the aging period progresses, the electrochemical kinetics gradually decrease inducing a loss in performance efficiency. The reduction in electrochemical active surface area (ECSA) can be attributed to the formation and accumulation of gas bubbles. With increasing aging time the contact angle evolves and bubbles tend to adhere to the electrode surfaces, resulting in a decrease in the available active surface area and hindered mass transport of reactants. Consequently, the electrochemical reactions are affected, leading to a decrease in electrochemical kinetics at the anode as noticeable in the **Figure 3**. Furthermore, the ion exchange overpotential tends to increase with time during the aging process as explained below. These changes introduce higher resistance to ion transport from liquid electrolyte to the ionomer-AEM interface, impeding the desired electrochemical reactions and resulting in an elevated ion exchange overpotential. As observed from the **Figure 4**, we see that the variation in the wettability properties of the PTL led to a variation in the relative permeability as well as the capillary

pressure at the electrodes with time. This reduction in the capillary pressure at the electrode leads to an induced difficulty in the evacuation of the gas bubbles that form at the electrode surface. As there is a continuing irreversible degradation in the wettability of the medium, these gas bubbles grow to reach a larger size and reducing the exchange current density at the electrode. The permanent loss in wettability is as a result to the reaction undergone by the Nickel with the supporting electrolyte used during the operation to form Nickel Hydroxide, which is comparatively less hydrophilic as compared to the metallic state. [21][23][24] Hence, this is a coupled effect, which is tantamount to both a reversible (bubble accumulation) and an irreversible degradation (oxide layer formation) mechanism.

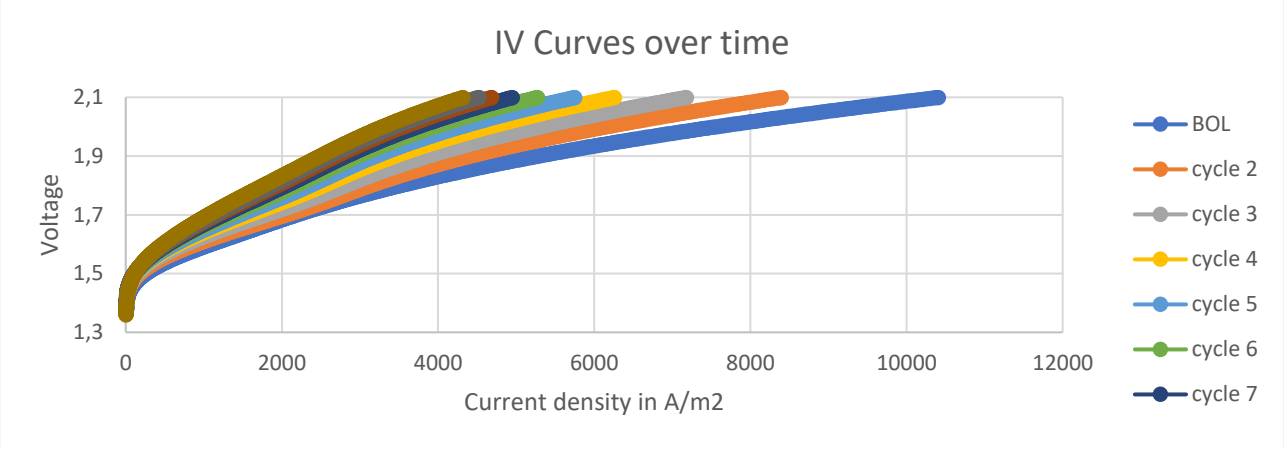

Figure 3 IV Curves evolution over aging operation period. Bol indicated IV curves recorded after 10 Hours, EOL indicates end of aging experiments at end of 100 Hours

The decrease in effective permeability of the wetting phase in the porous medium signifies a reduction in the flow capacity of the liquid component through the porous structure. In the **Figure 5**, the porous medium typically refers to the PTL (here a sinter). The wetting phase corresponds to the liquid, usually water or an aqueous electrolyte solution. The reduction in effective permeability indicates an increased resistance to the flow of the wetting phase within the porous medium. In the present work, we also compare the variation of overpotential that impact performance and their evolution with time. The model fitting using the IV curve cannot be done as can be observed in **Figure 6** only by tuning the contact angle and the associated transport properties. The evolution of them affect essentially the high current part of the curve while the small current part is affected by the electrochemistry. Thus, during the fitting process we had to modify also the ion exchange overpotential in order to obtain a good fitting. As can be seen in **Figure 7**, the ion exchange overpotential that occurs at the electrodes drastically increases over time and is substantially large at the end of operation. It suggests the possible reduction in the ion transport capability of the medium over extended periods of time.

3 Conclusion

The study of wettability loss in the Porous Transport Layer of an AEM-based water electrolyzer highlights its significant impact on the effective permeability and performance of the device. The presence of gas bubbles and changes in wettability contribute to reduce transport and distribution of the wetting phase. It is evident that the gas bubbles stagnation at the Gas diffusion electrodes is because of permanent loss of wettability due to oxidation of the sinter. Future research will focus on exploring degradation mechanisms in detail to develop strategies for mitigating wettability loss and improving overall electrolyzer performance. Detailed surface characterisation and post-mortem analysis have also been

scheduled for the future to better understand the impact and origin of aging mechanisms in the AEMWE.

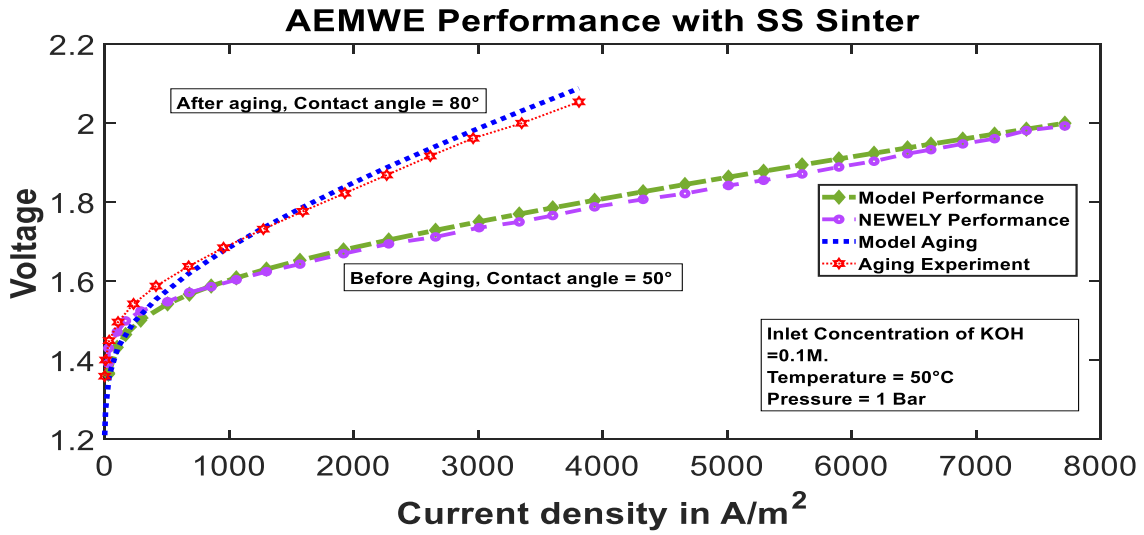

Figure 4 AEMWE performance at the beginning and end of the durability tests validated with the modified contact angle approach to study the wettability loss in an AEMWE

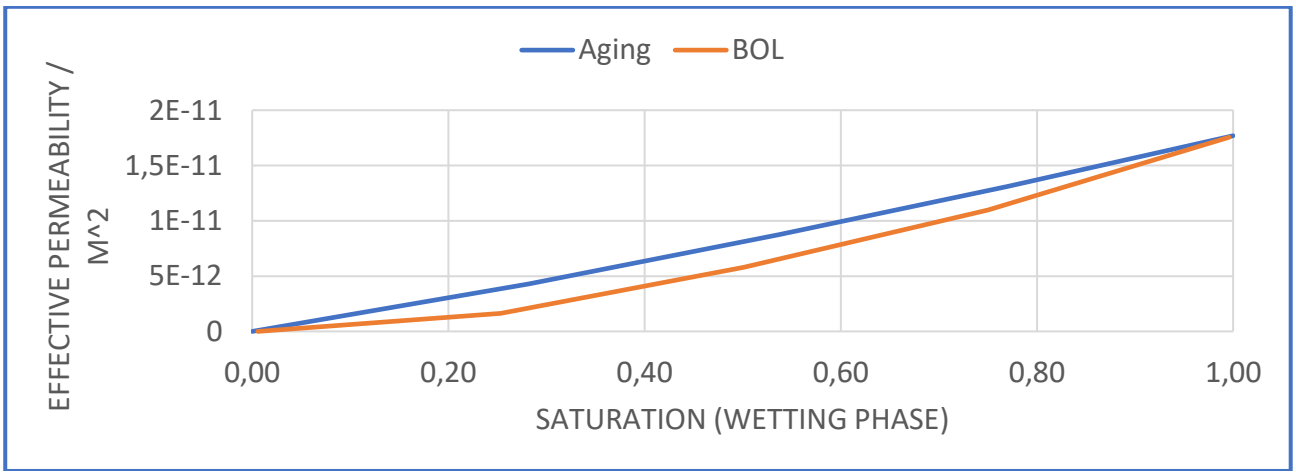

Figure 5 Evolution of the effective permeability of water in the sinter during BOL (After 10 Hours) and end of 100 Hours

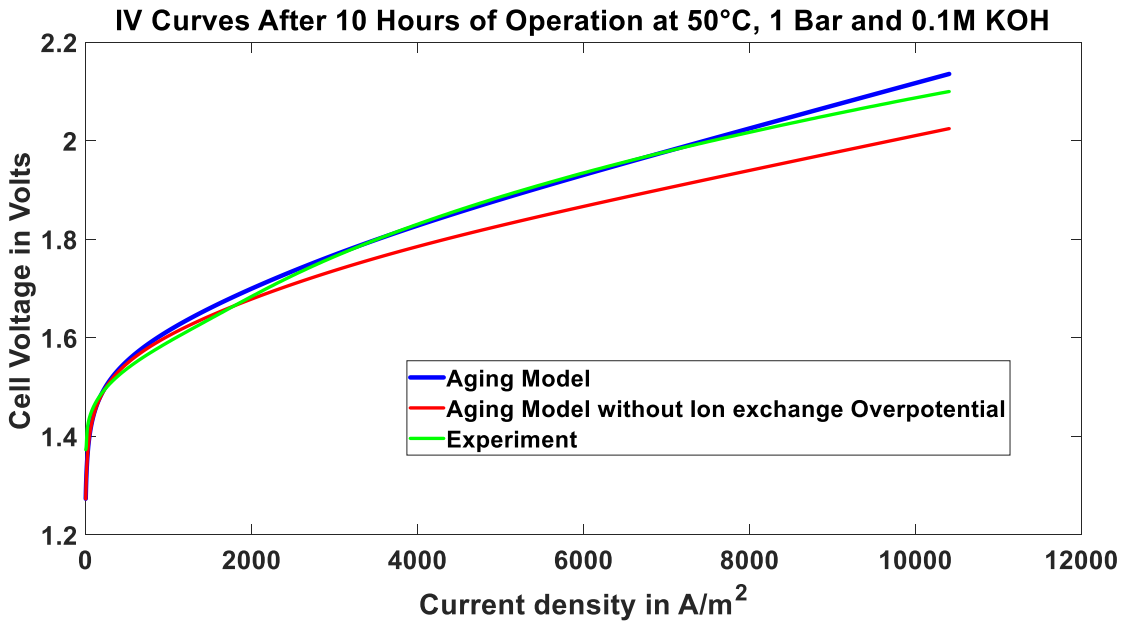

Figure 6 Fitting of the IV Curves obtained from experiments with and without including the Ion exchange overpotential term in the model.

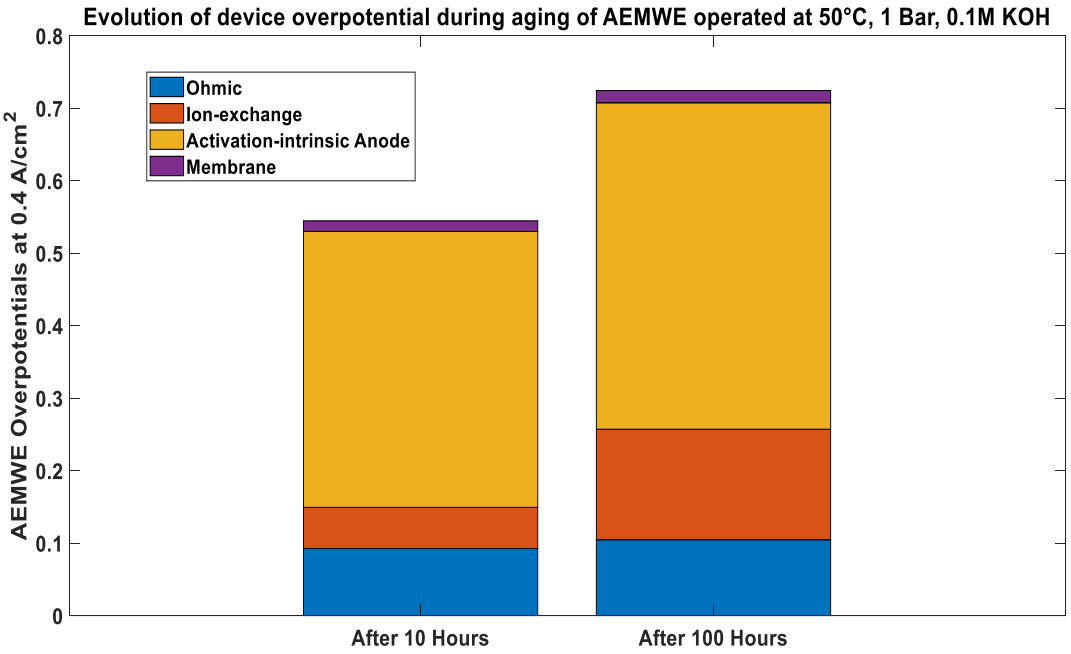

Figure 7 Overpotential of the AEMWE in Volt at 0.4 A/cm^2 after break-in device operation at 10 hour and end of extended aging tests. The pH overpotential and kinetics overpotential at the cathode was assumed constant along the operation.

ACKNOWLEDGMENT

THIS PROJECT HAS RECEIVED FUNDING FROM THE FUEL CELLS AND HYDROGEN 2 JOINT UNDERTAKING UNDER GRANT AGREEMENT NO 875118. THIS JOINT UNDERTAKING RECEIVES SUPPORT FROM THE EUROPEAN UNION'S HORIZON 2020 RESEARCH AND INNOVATION PROGRAM, HYDROGEN EUROPE AND HYDROGEN EUROPE RESEARCH.

References

[1] Kang, Zhenye, et al. "Effects of various parameters of different porous transport layers in proton exchange membrane water electrolysis." *Electrochimica Acta* 354 (2020): 136641.

[2] Nouri-Khorasani, Amin, et al. "Model of oxygen bubbles and performance impact in the porous transport layer of PEM water electrolysis cells." *International journal of hydrogen energy* 42.48 (2017): 28665-28680.

[3] Oh, Jeong Hyun, et al. "Self-supported electrodes to enhance mass transfer for high-performance anion exchange membrane water electrolyzer." *Chemical Engineering Journal* 460 (2023): 141727.

[4] Bao, D., Wang, L., Lv, H., Yang, F., Shi, Y., & Gu, S. (2017). Anion exchange membrane electrolysis for hydrogen production: A review. International Journal of Hydrogen Energy, 42(9), 6029-6047.

[5] R. K. Panda, G. Serre, F. Fouda-Onana, Y. Bultel and P. Schott, "Performance evaluation of the Anion exchange membrane based Water electrolysis," 2022 10th International Conference on Systems and Control (ICSC), Marseille, France, 2022, pp. 102-107, doi: 10.1109/ICSC57768.2022.9993826.

[6] Park, J., & Choi, J. (2019). Numerical analysis of ion transport in anion exchange membrane water electrolysis with consideration of Donnan equilibrium. International Journal of Hydrogen Energy, 44(16), 8318-8330.

[7] V. A. Shaposhnik. Walter Nernst and analytical chemistry. Journal of Analytical Chemistry, 63(2) :199–201, Feb 2008.

[8] Liso, V.; Savoia, G.; Araya, S.S.; Cinti, G.; Kær, S.K. Modelling and Experimental Analysis of a Polymer Electrolyte Membrane Water Electrolysis Cell at Different Operating Temperatures. *Energies* **2018**, *11*, 3273.

[9] Rho, K.H.; Na, Y.; Ha, T.; Kim, D.K. Performance Analysis of Polymer Electrolyte Membrane Water Electrolyzer Using OpenFOAM®: Two-Phase Flow Regime, Electrochemical Model. *Membranes* **2020**, *10*, 441.

[10] Chen, X., Chen, L., Li, Q., & Jensen, J. O. (2019). The Donnan effect in anion exchange membrane water electrolysis. Journal of Materials Chemistry A, 7(11), 6227-6237.

[11] Han, Y., Chen, L., & Li, Q. (2018). The impact of Donnan potential on anion exchange membrane water electrolysis. Electrochimica Acta, 283, 680-689. doi: 10.1016/j.electacta.2018.06.112.

[12] Pushkareva, I.V.; Solovyev, M.A.; Butrim, S.I.; Kozlova, M.V.; Simkin, D.A.; Pushkarev, A.S. On the Operational Conditions' Effect on the Performance of an Anion Exchange Membrane Water Electrolyzer: Electrochemical Impedance Spectroscopy Study. *Membranes* **2023**, *13*, 192.

[13] Han, Bo, et al. "Modeling of two-phase transport in proton exchange membrane electrolyzer cells for hydrogen energy." *International Journal of Hydrogen Energy* 42.7 (2017): 4478-4489.

[14] An, Liang, et al. "Mathematical modeling of an anion-exchange membrane water electrolyzer for hydrogen production." *international journal of hydrogen energy* 39.35 (2014): 19869-19876.

[15] Pushkareva, I.;Solovyev, M.; Butrim, S.;Kozlova, M.; Simkin, D.;Pushkarev, A. On the Operation Conditions Effect on the Anion Exchange Membrane Water Electrolyzer Performance: Electrochemical Impedance Spectroscopy Study. *Membranes* **2023**, *13*, 192.

[16] *ACS Appl. Mater. Interfaces* 2020, 12, 47, 52509–52526.

[17] Pärnamäe, R., et al. "Bipolar membranes: A review on principles, latest developments, and applications." *Journal of Membrane Science* 617 (2021): 118538.

[18] Yuan, Shu, et al. "Bubble evolution and transport in PEM water electrolysis: Mechanism, impact, and management." *Progress in Energy and Combustion Science* 96 (2023): 101075.

[19] Li, Dongguo, et al. "Durability of anion exchange membrane water electrolyzers." *Energy & Environmental Science* 14.6 (2021): 3393-3419..

[20] Cossar, Emily, et al. "The performance of nickel and nickel-iron catalysts evaluated as anodes in anion exchange membrane water electrolysis." *Catalysts* 9.10 (2019): 814.

[21] Surface Analysis on Wettability of Nickel Foams, Chiang Mai J. Sci. 2020; 47(5) : 1092-1101

[22] Pierozynski, Boguslaw, et al. "Kinetics of oxygen evolution reaction on nickel foam and platinum-modified nickel foam materials in alkaline solution." *Journal of Electroanalytical Chemistry* 847 (2019): 113194.

[23] Angeles-Olvera, Z.; Crespo-Yapur, A.; Rodríguez, O.; Cholula-Díaz, J.L.; Martínez, L.M.; Videa, M. Nickel-Based Electrocatalysts for Water Electrolysis. Energies 2022, 15, 1609.

[24] Corrosion behaviour of the nickel based materials in an alkaline solution for hydrogen evolution, January 2017, Indian Journal of Chemical Technology 24(1):88-92

Keywords: low temp water electrolyzer, AEM, wettability ,mechanical degradation, H_2,